Catalysis Science & Technology

Accepted Manuscript

ROYAL SOCIETY OF CHEMISTRY

www.rsc.org/catalysis

Improving Mass-Transfer in Controlled Pore Glasses as Supports for the Platinum-Catalyzed Aromatics Hydrogenation

M. Goepel[1], H. Kabir[1], C. Küster[1], E. Saraci[1], P. Zeigermann[2], R. Valiullin[2], C. Chmelik[2], D. Enke[1], J. Kärger[2], R. Gläser[1,]*

[1] *Institute of Chemical Technology, Universität Leipzig, Germany*

[2] *Institute of Experimental Physics I, Universität Leipzig, Germany*

* author to whom correspondence should be addressed,
e-mail: roger.glaeser@uni-leipzig.de

Abstract

The liquid-phase hydrogenation of toluene and other alkyl substituted benzene derivatives with different critical diameters was investigated over Pt-catalysts supported on spherical controlled pore glasses (CPGs) as model supports at 373 K in the batch mode. The effect of mass-transfer within the catalyst pores was studied by varying the pore width (4, 10, and 80 nm) and average grain size (18 µm – 150 µm) of the Pt/CPG catalysts. For toluene hydrogenation, internal mass-transfer limitations were absent (effectiveness factor > 90 %) only for catalysts with particle sizes below 25µm and pore widths ≤ 10 nm or with a pore width of 80 nm and particle sizes around 75 µm, respectively. Effective diffusion coefficients obtained from initial reaction rates via the Thiele concept, e.g., 2.8 10^{-10} m^2 s^{-1} for toluene over the catalyst with 10 nm pore width, were an order of magnitude lower than when determined by PFG-NMR. This difference was explained in terms of transport resistances such as surface barriers affecting the diffusivity assessment via the Thiele concept, while PFG-NMR measures intraparticle diffusion only.

Keywords: hydrogenation, liquid phase, toluene, mass-transfer, Pt-catalyst, controlled pore glass, PFG-NMR

1 Introduction

Hydrogenation reactions play an important role in many industrial heterogeneously catalyzed reactions such as the removal of hetero atoms from crude

oil fractions [1], the transformation of unsaturated to saturated (cyclic) hydrocarbons [2,3] the defunctionalization of biomass [4], the reduction of carbonyl [5] and nitro groups in organic subtrates [6] as well as the production of pharmaceuticals, fine and bulk chemicals [7]. Metal-catalyzed hydrogenation reactions are known to occur with high intrinsic reaction rates. Thus, the overall reaction rate is often limited by mass-transfer [8]. Therefore, the improvement of solid hydrogenation catalysts often depends on an understanding of the mass-transfer processes with respect to the catalytic conversion.

Generally, internal and external mass-transfer are distinguished. Internal mass-transfer refers to the transport of a reactant inside the catalyst pores. External mass transfer relates to reactant transport through the boundary layer around a catalyst particle, within the bulk phase surrounding the catalyst particles or across phase boundaries in multiphase reaction systems. Although a wealth of theoretical work was conducted in this field [9-11], systematic experimental catalytic investigations are less common. Most of the reported work was devoted to gas phase conversions [12], especially involving zeolite catalysts within which mass-transfer limitations may pose a crucial restriction for the reaction rates [13].

In recent years, materials with hierarchically structured pore systems (often zeolite based) generated interest due to their potential of overcoming mass-transfer limitations in heterogeneously catalyzed conversions [14-16]. These materials are most attractive due to the combination of the zeolitic micropores, providing a high surface area, and the larger pores (typically mesopores, d = 2–50 nm) providing improved accessibility to the micropores containing the majority of the catalytically active sites. Thus, the mesopores mainly act to supply mass-transfer routes within the catalyst particles resulting in an increased effectiveness factor. Several reports in this field attribute the higher catalytic activity to improved mass-transport in hierarchically structured pore systems [17-19]. It is, however, noteworthy that experimental data on the mass-transport in these catalytic systems are rarely presented. Moreover, knowledge about the required pore width for unhindered mass-transfer in the larger (meso)pores is needed to arrive at a rational design of hierarchically structured catalysts.

Particularly few experimental work is available on mass-transfer limitations of liquid-phase conversions. This is surprising in view of their industrial relevance, especially of catalytic liquid-phase hydrogenations [20], on the one hand, and in view of the fact that mass-transfer limitations are generally more likely to occur because of reduced diffusion rates in liquid compared to gaseous reaction phases, on the other hand. Although mass-transfer limitations were observed for catalytic liquid-phase conversions [20-22], systematic experimental investigations on how to overcome them are scarce. Recently, Foley et al. [23,24] conducted two studies on platinum supported on nanoporous carbon as a catalyst for the liquid-phase hydrogenation of different alkenes. Based on a study of the influence of mass-transfer, the catalyst design, i.e., grain size and porosity, was optimized to overcome internal mass-transfer limitations. However, in these carbon-based systems, the pore width cannot be readily adjusted. This results in broad or less-defined pore width distributions making correlations of mass-transfer behavior and pore width difficult.

In the present study, catalysts based on controlled pore glass (CPG) are presented as interesting alternative supports for metal-based hydrogenation catalysts. Controlled pore glasses are versatile catalyst support materials with tunable surface area, pore volume and narrow pore width distributions between 1-1000 nm [25]. They were already successfully used as catalyst supports [22,26] and are available as monoliths with different shapes including spheres [27]. They are, thus, interesting model supports for mass-transfer investigations.

Consequently, the aim of this study was to systematically investigate the influence of pore width and grain size of CPG-supported noble metal catalysts on the initial reaction rate in the hydrogenation of alkylated benzene derivatives as a model hydrogenation reaction. In particular, the mass-transfer properties and, ultimately, the pore width needed for unhindered mass-transfer during noble metal-catalyzed liquid-phase hydrogenations were determined. Thus, CPG spheres with pore widths between 4 and 100 nm were applied as supports for platinum as the catalytically active hydrogenation component.

Furthermore, the effective diffusion coefficients D_{eff} of the alkyl benzene reactants were determined from the effectiveness factor based on the Thiele concept.

The thus obtained D_{eff} values were, then, compared to an effective diffusion coefficient obtained by pulsed field gradient nuclear magnetic resonance (PFG-NMR) spectroscopy for a selected catalytic system. PFG-NMR is a well-established tool to directly measure effective diffusion coefficients [28-31], also applied for the selective measurement of the diffusivities of the individual components during catalytic reactions [32,33]. However, studies conducted under conditions similar to those of catalytic experiments (temperatures $\geq$ 373 K) are rare [34]. Thus, another aim of this study was to directly compare the diffusion coefficient obtained via PFG-NMR with the diffusion coefficient calculated using the Thiele concept applied to a catalytic conversion. This presents an attempt to experimentally verify the validity of the Thiele concept for determining effective diffusion coefficients under conditions of catalytic conversions.

2 Experimental section

2.1 Synthesis and characterization of the controlled pore glasses and supported Pt-catalysts

The spherical controlled pore glasses (CPGs) were synthesized according to the VYCOR-Process [25]. Therefore, non-porous glass beads (Biosearch Inc. Steinach, grain sizes 100 – 200 µm) with a composition of 70 wt.-% SiO_2, 23 wt.-% B_2O_3 and 7 wt.-% Na_2O were used to prepare CPGs with average pore widths of 4 (CPG(4)) and 10 nm (CPG(10)), respectively. To obtain a CPG with an average pore width of 80 nm (CPG(80)), an initial glass with a different composition, i.e., 62 wt.-% SiO_2, 30 wt.-% B_2O_3 and 7 wt.-% Na_2O and 1 wt.-% Al_2O_3, was used. First, an annealing (heating rate 10 K min^{-1}) was carried out for 24 h at different temperatures according to the desired pore widths, i.e., at 793 K for CPG(4), at 803 K for CPG(10), and at 863 K for CPG(80). Then, the solids were extracted, first with aqueous 3 N hydrochloric acid for 15 h at 363 K followed by treatment with an aqueous sodium hydroxide solution. While the extraction for CPG(4) and CPG(10) was carried out with 0.5 N sodium hydroxide solution for 1 h at room temperature, a three-step extraction was applied for

CPG(80), i.e., first for 4 h with 0.6 N, then twice with 0.4 N sodium hydroxide solution at 303 K for 2 h , respectively.

The CPG beads were loaded with platinum via electrostatic adsorption (EA). For that purpose, 10 g of the CPG beads were suspended in 50 cm³ deionized water. This suspension was kept at a pH of 10 via addition of 1 M aqueous ammonia solution (prepared using 32 wt.-% aqueous ammonia solution (≥ 30 wt.-% NH_3 content, Merck)) for 2 h under stirring. Afterwards, an aqueous solution of 0.1 M $Pt(NH_3)_4Cl_2 \cdot 2H_2O$ (3.52 g $Pt(NH_3)_4Cl_2 \cdot 2H_2O$ (99.0 Ma.-%, ABCR) dissolved in 100 cm³ deionized water) was added dropwise under stirring. After stirring for an additional hour, the solid was separated by filtration and washed three times with 20 cm³ deionized water. The complete removal of excess $Pt(NH_3)_4Cl_2$ from the support was proven by the absence of chloride ions in the washing water by addition of $AgNO_3$-solution. Finally, the solid was dried at 353 K overnight under an air atmosphere and reduced at 623 K for 4 h in a stream of 20 Vol.-% H_2 in N_2 (10 cm³ min^{-1}). The resulting catalysts were labelled Pt/CPG(4), Pt/CPG(10), and Pt/CPG(80), respectively, according to their average pore width. For the investigation of internal mass-transfer, the catalyst beads of Pt/CPG(4) and Pt/CPG(10) were crushed and sieved to obtain the grain size fractions of 0 – 50 µm, 51 –71 µm and 72 – 100 µm for Pt/CPG(4) and of 0 – 36 µm, 37 – 50 µm, 51 – 71 µm, 72 – 100 and 101 – 200 µm for Pt/CPG(10), respectively.

The characterization via N_2-sorption was conducted at 77 K using a micromeritics ASAP 2010 (for the catalysts Pt/CPG(4) and Pt/CPG(10)) and a Quantachrome Autosorb iQ (for the catalyst Pt/CPG(80)). Hg-intrusion was carried out using a Thermo Scientific, Pascal 440 Series instrument. Elemental analysis was achieved via optical emission spectrometry with inductively coupled plasma (ICP-OES, after microwave-assisted digestion of the samples in a mixture of 2.0 cm³ HF (48 %, Roth) 3.0 cm³ HNO_3 (69 %, Roth) and 3.0 cm³ HCl (35 %, Roth)) using a Perkin Elmer Optima 8000 instrument. Scanning electron microscopy (SEM) images of the catalysts were recorded on an E-O-GmbH CamScan CS44. Transmission electron microscopy (TEM) images were taken on a Philips CM-200 with an acceleration voltage of 200 kV. The detection limit for Pt-crystallites of the TEM

instrument used is about 1 nm. The catalyst density was determined using a micromeritics multivolume pycnometer 1305. X-ray powder diffraction (XRD) patterns were recorded on a Siemens D5000 diffractometer operating with Cu-Kα radiation (0.154 nm). The scanning range was 5-80° (2θ) using a step scan mode with the step of 0.05° (2θ). Hydrogen (Air Liquide, 99.999 %) chemisorption experiments were conducted using a Quantachrome Autosorb iQ in the vacuum volumetric mode at 313K. The isotherms for the dispersion calculation are given in the ESI, Figs. 5 and 6.

2.2 Catalytic experiments

The catalytic hydrogenation of aromatics was carried out in the batch mode using a stainless steel autoclave (Berghof, BR-200, volume = 200 cm^3, tetrafluoroethylene-coated) at 373 K, 1300 min^{-1} stirring speed and a static hydrogen pressure of 50 bar. As a reactant solution, a mixture of the aromatic (1.60 mol l^{-1}) and n-octane (0.19 mol l^{-1}, as internal standard for GC analysis, ≥ 98 %, Sigma-Aldrich) dissolved in n-hexane (≥ 95 %, VWR) was used. As aromatic reactants, toluene (≥ 99.5 %, Sigma Aldrich), m-xylene (99 %, Sigma-Aldrich), mesitylene (≥ 98.0, Merck Schuchardt) and 1,3,5-triisopropylbenzene (TIPB, 95 % Sigma-Aldrich) were used without further purification. The catalysts were reduced prior to use in an H_2/N_2 flow as described above. A typical catalytic experiment was performed by heating up the reactant solution (75 cm^3) and the suspended catalyst (150 mg) in the reaction autoclave up to 373 K. The reaction was, then, started by applying a static hydrogen pressure of 50 bar. Samples (0.5 cm^3) were taken periodically from the liquid reaction mixture through a sampling tube and the catalyst was separated by filtration. The product composition was analyzed using a GC (Shimadzu, 14 A) equipped with an FID (separation column: Macherey-Nagel, Optima 5, length: 30 m, inner diameter: 0.25 mm, film thickness: 0.25 µm).

The conversion of the aromatic reactants X_{aromatic} was calculated based on the aromatics concentration at time t ($c_{aromatic,t}$) and the initial aromatics concentration at time 0 ($c_{aromatic,0}$) using the equation

$$X_{aromatic} = \frac{(c_{aromatic,0} - c_{aromatic,t})}{c_{aromatic,0}} \cdot 100\ \%. \quad (1)$$

The experimental accuracy of the conversion data is ± 8 % of the reported value. The carbon balance was closed within 98 %. No coke formation or side products were observed.

2.3 Pulsed field gradient nuclear magnetic resonance measurements

For the pulsed field gradient nuclear magnetic resonance (PFG-NMR) experiments, a solution of 1.60 mol l^{-1} toluene dissolved in d-14 n-hexane (Merck Millipore, > 99% deuterated) was added to the reduced Pt/CPG(10) in a glass ampule. The amount of the liquid (d-14 n-hexane and toluene) was chosen to provide complete filling with the capillary-condensed liquid of the mesopore space only. Therefore, an excess amount of the d-14 n-hexane-toluene mixture was added to Pt/CPG(10) into the glass ampule. The ampule was then shaken and left to equilibrate for 5 min. Afterwards, the excess solution was removed using a syringe. The interparticle space remained filled with the vapor phase. Thereafter, the glass tube was sealed keeping the bottom part of the tube containing the catalyst particles at liquid nitrogen temperature.

The ^{1}H diffusion measurements were performed with an NMR spectrometer operating at a proton resonance frequency of 400 MHz, equipped with a home-built pulsed field gradient unit with field gradient amplitudes up to 35 T m^{-1} [35]. This means that only toluene molecules were traced in the experiments. For minimizing disturbing effects due to internal field gradients and eddy currents, the 13-interval stimulated-echo pulse sequence with bipolar gradients was applied [36].

Typical experimental parameters were δ = 400 μs for the gradient pulse width, 1.2 ms for the pulse separations within a pair of bipolar gradient pulses. The observation time, i.e., the separation t_d between the two gradient pulse pairs, was varied between 10 and 100 ms. The primarily measured spin-echo diffusion attenuation functions, which were obtained by varying the gradient strength g^2 keeping all other parameters constant, were found to have exponential shape. In addition, when plotted versus $(\gamma\delta g)^2 t_d$, where γ is the gyromagnetic ratio for protons, the echo

attenuations were found to be independent of the observation time t_d. These two facts revealed that, in this way, no disturbing boundary effects were present during measurements and the genuine intraparticle diffusivities were measured.

3 Results and discussion

3.1 Pt Catalysts supported on CPG beads

Three catalysts containing comparable Pt contents on controlled pore glasses (CPGs) were prepared. The three catalysts possess comparable specific surface areas, but different pore widths and, thus, different specific pore volumes as can be seen from the nitrogen sorption isotherms (Fig. 1). A relatively narrow pore width distribution with a maximum at 4 nm and 10 nm was found for the catalysts Pt/CPG(4) and Pt/CPG(10), respectively (Fig. 2). The pore width distribution of the catalyst Pt/CPG(80) as determined via Hg-intrusion is broader with a well pronounced maximum at ca. 80 nm (Fig. 3). The pore width maximum calculated from the nitrogen sorption isotherm is, however, somewhat lower, i.e., around 70 nm (Fig. 2). Inaccuracies of the pore size characterization of macroporous solids via nitrogen sorption are well known and are mostly attributed to the capillary condensation occurring close to the saturation pressure of nitrogen. To ensure comparability of the textural data obtained, Hg-intrusion measurements were also conducted on the catalysts Pt/CPG(4) and Pt/CPG(10) (ESI, Figs. 1 and 2). The data obtained via Hg-intrusion agree reasonably well with those from N_2-sorption. The textural properties of the catalysts are summarized in Table 1. The materials exhibit a spherical macroscopic shape with a narrow size distributions around 150-200 µm for the catalysts Pt/CPG(4) and Pt/CPG(10) and 50-100 µm for the catalyst Pt/CPG(80), respectively (Fig. 4).

Furthermore, all catalysts possess a similar Pt-loading of around 2.2 wt.-% (Table 1). No Pt reflections are observed in the XRD patterns for all catalysts investigated (ESI,

Fig 3). Assuming a detection limit of 5 nm for XRD , a Pt dispersion of >25 % is calculated [22,37]. In addition, TEM analysis was conducted for the catalyst Pt/CPG(10) (SEM overview: ESI, Fig. 4). However, no Pt particles can be detected by TEM. Considering the detection limit for Pt-crystallites of the TEM instrument used (ca. 1 nm), the Pt dispersion is >85 % assuming ideally spherical particles [37]. These findings are further supported by the results from hydrogen chemisorption for the catalysts Pt/CPG(10) and Pt/CPG(80) (for isotherms see ESI, Figs. 5 and 6). Accordingly, a Pt dispersion of 91 % and 87 % was determined for Pt/CPG(10) and Pt/CPG(80), respectively. These values correspond to the same Pt dispersion within experimental accuracy of hydrogen chemisorption.

3.2 Toluene hydrogenation

To investigate for possible mass-transfer limitations, the CPG-supported Pt catalysts were used in the liquid-phase hydrogenation of toluene. A clear correlation between the average pore width (d_{pore}) and the conversion as a function of time can be seen for the three catalysts (Fig. 5). Thus, the catalyst with the largest average pore width (Pt/CPG(80)) shows the fastest toluene conversion. For the catalysts with the smaller pore widths, the toluene conversion is slower. As a measure for the catalyst performance in the hydrogenation reactions, the initial reaction rate, determined as the slope of the linear part of the dependence of conversion on time at the beginning of the experiments, was used. As the linear dependence of conversion over reaction time extends over the whole reaction duration studied (up to 200 min, or until complete conversion was reached), a deactivation of the catalyst during the experiment can be excluded. Since the Pt loading and dispersion are comparable, the higher initial reaction rate for the catalysts with larger pore widths (Pt/CPG(4): 0.032 mmol g^{-1} s^{-1}, Pt/CPG(10) 0.060 mmol g^{-1} s^{-1} and Pt/CPG(80): 0.144 mmol g^{-1} s^{-1}) is an indication for higher internal mass-transfer rates within the respective catalyst pore systems.

The reaction rate for Pt/CPG(10) can be calculated on basis of the reaction rate of Pt/CPG(4) using the Thiele concept and assuming internal mass-transfer limitation and Knudsen diffusion (for detailed calculation see ESI). This calculated reaction rate

value for Pt/CPG(10) (0.051 mmol g^{-1} s^{-1}) is in good agreement with the one determined experimentally (0.060 mmol g^{-1} s^{-1}). Evidently, the assumption of mass-transfer limitation in case of Pt/CPG(4) and Pt/CPG(10) for the toluene hydrogenation is valid. Note, however, that Knudsen diffusion is usually related to mass-transfer in porous solids with a surrounding gas-phase. It apparently describes the diffusion under the liquid-phase conditions of the present reaction systems equally well.

The absence of external mass-transfer limitations, i.e., hindered mass-transfer of hydrogen from the gas into the liquid phase, inside the bulk liquid phase and from the liquid phase through the boundary layer to the outer catalyst surface, was investigated in a separate series of experiments varying the stirring speed (see ESI, Fig. 7). At values above 600 min^{-1}, the initial reaction rate of toluene was independent of the stirring rate proving the absence of external mass-transfer limitations. Consequently, all further conversions were carried out at a stirring speed of 1300 min^{-1} to exclude limitations by external mass transfer.

3.2.1 Influence of the catalyst grain size

In order to investigate the role of internal mass-transfer limitation in more detail, a variation of the average grain size was performed for the catalysts Pt/CPG(4) and Pt/CPG(10). Upon increasing the average grain size, the observed initial reaction rate decreases for both catalysts (Fig. 6). This again indicates the occurrence of internal mass-transfer limitation, since the diffusion pathway is longer in larger catalyst grains. Note that the reaction is apparently limited by internal mass transfer over the whole grain size range studied. Furthermore, for average grain sizes smaller than 25 µm, the initial reaction rates for Pt/CPG(4) and Pt/CPG(10) are comparable. This can be understood, since at this average grain size the influence of the internal mass-transfer on the reaction rate is negligible and, thus, the intrinsic reaction on the Pt-particles dominates the observed initial rate and is independent of mass transfer. Because of the similar Pt-content and -dispersion, these intrinsic reaction rates are expected to be similar for both catalysts. On the other hand, the comparable reaction rates over the two catalysts can be seen as an indication for a comparable local distribution of the Pt-particles inside the catalyst grains. Note also that the slope of the rate decrease with

increasing average grain size is steeper for the catalyst Pt/CPG(4) with the smaller pore width than for Pt/CPG(10). This is, again, consistent with the expected limitation of the observed reaction rate by mass transfer within the catalyst pores.

3.2.2 Calculation of Thiele modulus and effectiveness factor

Based on the results of the grain size variation (Fig. 6), the Thiele modulus and the effectiveness factor for each catalyst were calculated according to the literature[38]. Based on the Weisz-Prater-Criterion (C_{wp}), the Thiele modulus (θ) and the effectiveness factor (η) can be put in relation with the observed initial reaction rate r_0 according to

$$C_{WP} = \eta\,\theta^2 = \frac{r_0\,\rho\,d_{grain}^2}{D_{eff}c_{surf}} = 3(\theta\,coth\,\theta - 1), \qquad (2)$$

where ρ is the catalyst density, d_{grain} is the grain size, D_{eff} is the effective diffusion coefficient and c_{surf} the toluene concentration at the outer catalyst surface. If no external mass-transfer limitations occur (as proven by the stirring speed variation, cf. section 3.2 and ESI, Fig. 3), the toluene concentration on the outer surface of the catalyst (c_{surf}) can be assumed to be equal to the bulk concentration, i.e., 1.60 mol l^{-1}. If equation (2) is applied to two catalytic experiments (with the subscripts 1 and 2), in which only the grain size of the catalyst is varied, the ratio of these two equations is

$$\frac{r_{0,2}d_{grain,2}}{r_{0,1}d_{grain,1}} = \frac{\theta_2\,coth\,\theta_2 - 1}{\theta_1\,coth\,\theta_1 - 1}. \qquad (3)$$

Note that the terms c_{surf}, ρ, D_{eff} cancel because they are assumed to be identical for two catalytic experiments under the same conditions. According to the literature[38], the Thiele modulus (with r_{int} as the intrinsic, i.e. not mass-transfer limited reaction rate) can be defined as

$$\theta = d_{grain}\sqrt{\frac{r_{int}\,\rho}{D_{eff}c_{surf}}}\,. \quad (4)$$

Thus, for the ratio of the Thiele moduli for the two experiments, we obtain

$$\theta_1 = \frac{d_{grain,1}}{d_{grain,2}}\theta_2. \quad (5)$$

Substituting equation (5) in equation (3) results in

$$\frac{r_{0,2}d_{grain,2}}{r_{0,1}d_{grain,1}} = \frac{\theta_2\,coth\,\theta_2 - 1}{\frac{d_{grain,1}}{d_{grain,2}}\theta_2\,coth\frac{d_{grain,1}}{d_{grain,2}}\theta_2 - 1}. \quad (6)$$

This equation can be numerically solved to obtain the Thiele modulus θ_2. θ_1 can then be calculated from equation (5). The effectiveness factor η and the effective diffusion coefficient D_{eff} are calculated using equation (2) (ρ = 2.1 g cm^{-3}).

As Fig. 7 shows, an effectiveness factor of about 90 % is reached for both catalysts Pt/CPG(4) and Pt/CPG(10), when the average grain size is below 25 µm. The differently strong influence of the mass-transfer limitation on the conversion over the catalysts Pt/CPG(4) and Pt/CPG(10) is indicated by the different slopes of the decrease of the effectiveness factor with average grain size. This decrease is more pronounced for Pt/CPG(4) than for Pt/CPG(10), consistent with the earlier conclusion drawn from the dependence of the initial reaction rate of average grain size (see Fig. 6). Consequently, the effective diffusion coefficients calculated for Pt/CPG(4) (D_{eff} = 0.8 · 10^{-10} m^2 s^{-1}) is about three times lower than that of Pt/CPG(10) (D_{eff} = 2.8 · 10^{-10} m^2 s^{-1}).

3.3 Hydrogenation of alkyl substituted benzene derivatives

As another important parameter of the mass-transport inside a pore network, the dimension (size) of the reactant molecule needs to be considered. Therefore, the catalytic hydrogenation of alkyl substituted benzene derivatives with different critical

diameters d_{crit} was studied, i.e., methyl-benzene (toluene, d_{crit} = 0.67 nm [39]), 1,3-dimethylbenzene (m-xylene, d_{crit} = 0.74 nm [39]), 1,3,5-trimethylbenzene (mesitylene, d_{crit} = 0.82 nm [40]) and 1,3,5-triisopropylbenzene (TIPB, d_{crit} = 0.95 nm [41]) (reaction scheme: Fig. 8). The critical diameter d_{crit} is defined as the smallest cylindrical orifice through which a molecule can pass [42].

The results of the hydrogenation of these reactants using the catalysts Pt/CPG(10) and Pt/CPG(80) are displayed in Fig. 9. As already discussed above (cf. Fig. 5), the hydrogenation of toluene proceeds with an about three-fold higher initial reaction rate when using the catalyst with the larger average pore width of 80 nm (Pt/CPG(80)) instead of the one with 10 nm pore width (Pt/CPG(10)). This higher initial reaction rate was attributed to faster internal mass-transfer within the Pt/CPG(80) catalyst compared to the catalyst Pt/CPG(10). Moreover, the initial reaction rate for toluene hydrogenation over Pt/CPG(80) is essentially the same as that for the catalysts with the smaller pore widths, i.e., Pt/CPG(10) and Pt/CPG(4), and an average grain size of 25 µm (Fig. 6, ca. 0.15 mmol g^{-1} s^{-1}). This indicates that the reaction rate of toluene is not limited by internal mass transfer on Pt/CPG(80). As mentioned above, the similar reaction rates provide further evidence for a comparable local distribution of the Pt-particles inside the catalyst grains. Also for the other alkyl substituted benzenes, the initial reaction rate is generally higher by a factor of 2 to 4 over Pt/CPG(80) than over Pt/CPG(10). Note, however, that the pore width of both catalysts is larger by at least on order of magnitude than the critical molecule diameter of all reactants studied.

The decrease in initial reaction rate with increasing critical molecule diameter of the reactant is almost linear for both catalysts, with the initial rate for TIPB conversion over Pt/CPG(80) being the only exception. This clearly reflects the growing impact of mass transfer on the observed reaction rate with increasing critical molecule diameter. For toluene and m-xylene no, or only small mass-transfer limitations are expected. With increasing critical molecule diameter, the influence of mass transfer becomes more pronounced, severely limiting the initial reaction rate. Interestingly, the slopes for the linear decrease of the initial reaction rate with increasing critical molecule diameter is similar for both catalysts (Fig. 9). This indicates that the same mode of mass transfer takes place in the pores of both catalysts. It is, however, surprising that

the slope is not steeper for the catalyst with the smaller pores (Pt/CPG(10)) which might be expected for stronger limitations of the mass transfer within the grains of this catalyst. A possible explanation for this finding is that the initial reaction rates for Pt/CPG(10) are closer to the threshold reaction rate for an effectiveness factor (η) $\rightarrow$ 0 corresponding to the conversion taking place at the outer surface of the catalyst only. Thus, the reaction rate is less strongly affected by slower mass-transport of the bulkier molecules.

When considering the decrease of the initial reaction rate of the alkyl substituted benzenes with increasing critical diameter of the reactant molecules, the intrinsic reaction rate needs to be taken into account. The adsorption of aromatics on noble metal surfaces is known to occur via π-bonding involving electron transfer from the aromatic ring to the unoccupied d-orbitals of the noble metal atoms [43]. Since the π-electron density in aromatics increases with increasing degree of alkyl-substitution, the aromatic reactants are expected to bind more strongly. This was confirmed by Gallezot et al. [44] for the adsorption of benzene and toluene on Pt(111) surfaces Smith et al. [45] observed similar reaction rates for the hydrogenation of toluene, m-xylene and mesitylene using a platinum catalysts under similar reaction conditions (liquid phase, solvent: acetic acid, aromatics concentration 0.2 mol l^{-1}, 303 K). However, it is to be expected that a higher reaction rate results for more electron rich aromatics, i.e., with higher degree of alkylation. Thus, the decreasing reaction rates with increasing molecular diameter of the aromatic reactants as observed here (Fig. 8) is in line with an increasing mass-transfer limitation within the catalysts pores.

3.4 Pulsed field gradient nuclear magnetic resonance

For the catalyst Pt/CPG(10), the effective diffusion coefficient was determined using PFG-NMR at temperatures between 313 K and 373 K (Fig. 10). For 373 K, the temperature of the catalytic experiments (cf. above), the effective diffusion coefficient D_{eff} determined via PFG-NMR amounts to $35 \cdot 10^{-10}$ m^2 s^{-1}. This is about one order of magnitude larger than the effective diffusion coefficient calculated using the Thiele concept from the initial catalytic reaction rates ($2.9 \cdot 10^{-10}$ m^2 s^{-1}). The difference in

D_{eff} may be attributed to the fact, that the PFG-NMR measurement was, due to experimental reasons, not conducted under a static hydrogen pressure of 50 bar as applied in the catalytic experiments. Because of the low solubility of hydrogen in n-hexane [46], the static pressure of 50 bar mainly results in a compression and, thus, a density increase of the liquid n-hexane. However, the density of toluene increases only by 1 % upon a pressure increase of 50 bar [47]. In addition, toluene can be assumed to be a hard sphere fluid [48], the diffusivity and density of which are indirectly proportional. Thus, a tenfold decrease of D_{eff} cannot be explained by the increased pressure.

Consequently, the higher values of the effective diffusivities determined by PFG-NMR might be related to the existence of an additional transport resistance at the particle surface ("surface barriers"), giving rise to a finite surface permeability. The surface permeability is defined as the factor of proportionality between the flux through the surface and the concentration difference between actual concentration in the genuine pore space close to the surface and the pore space concentration in equilibrium with the bulk liquid-phase reactant concentration [49]. The relevance of these surface permeabilities concerning mass-transfer processes was proven in different studies [50,51] and was recently summarized in a review [49].

When D_{eff} is determined on the basis of the Thiele concept, it is assumed, that the deviation of the observed initial reaction rate from the intrinsic reaction rate is only based on the slower rate of mass-transfer through the pore system with respect to the reaction at the catalytically active sites. If, however, the surface permeability of the investigated system is low, i.e., if mass-transfer through the surface (not the external boundary layer, cf. section 3.2 and ESI, Fig. 3) is hindered, the observed reaction rate will also be decreased. The Thiele concept does not take into account surface permeabilities, and, thus, the decrease in the initial reaction rate observed is only attributed to a slower mass-transfer inside the pore system. This results in an underestimation of the diffusion coefficient. However, in PFG-NMR, the experimental conditions (observation time and grain size) are chosen so that the diffusion of the molecules of interest are only observed within the pore system and not entering or leaving the pore system. As a consequence, the D_{eff} determined by PFG-NMR will not be falsified by surface permeability effects. It can furthermore be concluded that,

although the Thiele modulus can be applied to obtain an estimate of D_{eff}, even if the surface permeability of an investigated catalyst is low, the D_{eff} calculated using the Thiele concept will always be lower than the real value.

4 Conclusions

Mass-transfer effects in liquid-phase hydrogenation reactions of alkyl substituted aromatics were investigated over Pt catalysts supported on controlled pore glasses (CPGs) as suitable model supports. These supports are available as monoliths with adjustable pore widths in the range of 1-1000 nm. For three different CPGs with spherical particles of 80 and 200 µm diameter and pore widths between 4 and 80 nm as well as a Pt-loading of 2 wt.-%, it was shown that aromatics hydrogenation under typical conditions can be mass-transfer limited, even for larger mesopores around 80 nm.

While for catalyst particles with 25 µm diameter (and for 80 nm pore width), toluene conversion occurrs with the intrinsic (kinetic) reaction rate, the conversion of reactants with bulkier molecules such as m-xylene or mesitylene, is evidently hindered by internal mass-transfer within the catalyst mesopores. Evidently, an average pore width of at least 80 nm is needed to overcome internal mass-transfer limitations in the liquid-phase hydrogenation of toluene (d_{crit} = 0.61 nm), corresponding to a ratio of average pore width to critical molecule diameter of about 130. This knowledge may serve as a guide for a rational design of mass-transfer optimized hierarchical hydrogenation catalysts in the future.

Moreover, a particle size reduction may be applied to avoid mass-transfer limitations. Thus, for catalysts with mesopores of 10 nm, to achieve effectiveness factors $\geq$ 0.9 in toluene hydrogenation, the particle size would have to be below 25 µm, which is in the range of fine powders. If catalyst particles of larger diameters are to be applied, the only option for prohibiting mass-transfer-limited conditions for

liquid-phase hydrogenations is, thus, to introduce sufficiently large pores, ideally with widths of 100 nm or beyond.

The effective diffusion coefficient of toluene for the catalysts with 4 and 10 nm pore width was determined from the initial reaction rates using the Thiele concept. The diffusion coefficient obtained from PFG-NMR is, however, an order of magnitude larger. Apparently, the Thiele concept is too simplified to assess the intraparticle transport of the reactants only. Rather, additional transport hindrances such as surface barriers may affect the diffusivity determination via the Thiele concept. It presents a challenge for further studies to identify more precisely these additional phenomena influencing diffusivity determination under conditions of catalytic reactions.

Acknowledgements

The authors would like to thank the "Deutsche Forschungsgemeinschaft" for funding within the International Research Training Group GRK 1056 "Diffusion in Porous Materials".

5 References

[1] Song, C. S. *Catal. Today* **2003**, *86*, 211.
[2] Blaser, H. U.; Malan, C.; Pugin, B.; Spindler, F.; Steiner, H.; Studer, M. *Adv. Synth. Catal.* **2003**, *345*, 103.
[3] Willis, M. C. *Chem. Rev.* **2010**, *110*, 725.
[4] Sutton, A. D.; Waldie, F. D.; Wu, R. L.; Schlaf, M.; Silks, L. A.; Gordon, J. C. *Nat. Chem.* **2013**, *5*, 544.
[5] Bonnemann, H.; Brijoux, W.; Tilling, A. S.; Siepen, K. *Top. Catal.* **1997**, *4*, 217.
[6] Lou, X. B.; He, L.; Qian, Y.; Liu, Y. M.; Cao, Y.; Fan, K. N. *Adv. Synth. Catal.* **2011**, *353*, 281.
[7] Chen, B.; Dingerdissen, U.; Krauter, J. G. E.; Rotgerink, H. G. J. L.; Mobus, K.; Ostgard, D. J.; Panster, P.; Riermeier, T. H.; Seebald, S.; Tacke, T.; Trauthwein, H. *Appl. Catal. A-Gen.* **2005**, *280*, 17.
[8] Tadepalli, S.; Lawal, A. *Int. J. Chem. React. Eng.* **2008**, *6*.
[9] Rao, S. M.; Coppens, M. O. *J. Phys. Chem. C* **2012**, *116*, 26816.
[10] Wang, G.; Coppens, M. O. *Ind. Eng. Chem. Res.* **2008**, *47*, 3847.
[11] Wang, G.; Johannessen, E.; Kleijn, C. R.; de Leeuwa, S. W.; Coppens, M. O. *Chem. Eng. Sci.* **2007**, *62*, 5110.
[12] Tang, T. D.; Yin, C. Y.; Wang, L. F.; Ji, Y. Y.; Xiao, F. S. *J. Catal.* **2007**, *249*, 111.
[13] Christensen, C. H.; Johannsen, K.; Schmidt, I.; Christensen, C. H. *J. Am. Chem. Soc.* **2003**, *125*, 13370.

[14] Christensen, C. H.; Johannsen, K.; Toernqvist, E.; Schmidt, I.; Topsoe, H.; Christensen, C. H. *Catal. Today* **2007**, *128*, 117.
[15] Holm, M. S.; Taarning, E.; Egeblad, K.; Christensen, C. H. *Catal. Today* **2011**, *168*, 3.
[16] Perez-Ramirez, J.; Christensen, C. H.; Egeblad, K.; Christensen, C. H.; Groen, J. C. *Chem. Soc. Rev.* **2008**, *37*, 2530.
[17] Liu, B. Y.; Zheng, L. M.; Zhu, Z. H.; Li, C.; Xi, H. X.; Qian, Y. *Appl. Catal. A-Gen.* **2014**, *470*, 412.
[18] Zheng, J. J.; Zeng, Q. H.; Yi, Y. M.; Wang, Y.; Ma, J. H.; Qin, B.; Zhang, X. W.; Sun, W. F.; Li, R. F. *Catal. Today* **2011**, *168*, 124.
[19] Wang, D. J.; Liu, Z. N.; Wang, H.; Xie, Z. K.; Tang, Y. *Micropor. Mesopor. Mater.* **2010**, *132*, 428.
[20] Rautanen, P. A.; Aittamaa, J. R.; Krause, K. O. I. *Ind. Eng. Chem. Res.* **2000**, *39*, 4032.
[21] Wilde, N.; Worch, C.; Suprun, W.; Gläser, R. *Micropor. Mesopor. Mater.* **2012**, *164*, 182.
[22] Goepel, M.; Al-Naji, M.; With, P.; Wagner, G.; Oeckler, O.; Enke, D.; Gläser, R. *Chem. Eng. Technol.* **2014**, *37*, 551.
[23] Peer, M.; Qajar, A.; Holbrook, B. P. M.; Rajagopalan, R.; Foley, H. C. *Carbon* **2013**, *57*, 485.
[24] Holbrook, B. P. M.; Rajagopalan, R.; Dronvajjala, K.; Choudhary, Y. K.; Foley, H. C. *J Mol. Catal. A-Chem.* **2013**, *367*, 61.
[25] Enke, D.; Janowski, F.; Schwieger, W. *Micropor. Mesopor. Mater.* **2003**, *60*, 19.
[26] Stolle, A.; Schmoger, C.; Ondruschka, B.; Bonrath, W.; Keller, T. F.; Jandt, K. D. *Chinese J. Catal.* **2011**, *32*, 1312.
[27] Munkelt, T.; Kuster, C.; Hamel, C.; Enke, D.; Seidel-Morgenstern, A. *Chem. Ing. Tech.* **2013**, *85*, 1686.
[28] Mehlhorn, D.; Valiullin, R.; Kärger, J.; Cho, K.; Ryoo, R. *Materials* **2012**, *5*, 699.
[29] Chmelik, C.; Karger, J. *Chem. Soc. Rev.* **2010**, *39*, 4864.
[30] Kärger, J; Ruthven, D. M.; Theodorou D. N. *Diffusion in Nanoporous Materials*; Wiley - VCH: Weinheim, 2012.
[31] Kärger, J.; Valiullin, R. *Chem. Soc. Rev.* **2013**, *42*, 4172.
[32] Hong, U.; Kärger, J.; Hunger, B.; Feoktistova, N. N.; Zhdanov, S. P. *J. Catal.* **1992**, *137*, 243.
[33] Schwarz, H. B.; Ernst, S.; Kärger, J.; Knorr, B.; Seiffert, G.; Snurr, R. Q.; Staudte, B.; Weitkamp, J. *J. Catal.* **1997**, *167*, 248.
[34] Heink, W.; Karger, J.; Pfeifer, H.; Datema, K. P.; Nowak, A. K. *J. Chem. Soc. Faraday T.* **1992**, *88*, 3505.
[35] Galvosas, P.; Stallmach, F.; Seiffert, G.; Kärger, J.; Kaess, U.; Majer, G. *J. Magn. Reson.* **2001**, *151*, 260.
[36] Wu, D. H.; Chen, A. D.; Johnson, C. S. *J. Magn. Reson. Ser. A* **1995**, *115*, 260.
[37] Gallezot, P.; Bergeret, G. In *Handbook of Heterogenous Catalysis*; Ertl, G.; Knözinger, H.; Schüth, F.; Weitkamp J. (Eds.); Wiley-VCH: Weinheim, Germany, 2008.
[38] Fogler, H. S. *Elements of Chemical Reaction Engineering*; 4th edition ed.; Prentice Hall PTR, Westford, 2006.
[39] Choudhary, V. R.; Nayak, V. S.; Choudhary, T. V. *Ind. Eng. Chem. Res.* **1997**, *36*, 1812.
[40] Webster, C. E.; Drago, R. S.; Zerner, M. C. *J. Phys. Chem. B* **1999**, *103*, 1242.
[41] Al-Khattaf, S.; de Lasa, H. *Appl. Catal. a-Gen.* **2002**, *226*, 139.
[42] Zaman, S. F.; Loughlin, K. F.; Al-Khattaf, S. S. *Ind. Eng. Chem. Res.* **2005**, *44*, 2027.
[43] Rooney, J. J. *J. Mol. Catal.* **1985**, *31*, 147.
[44] Massardier, J.; Bertolini, J. C.; Tri, T. M.; Gallezot, P.; Imelik, B. *B. Soc. Chim. Fr.* **1985**, 333.
[45] Rader, C. P.; Smith, H. A. *J. Am. Chem. Soc.* **1962**, *84*, 1443.
[46] Gao, W. Z.; Robinson, R. L.; Gasem, K. A. M. *J. Chem. Eng. Data* **2001**, *46*, 609.

[47] McLinden, M. O.; Splett, J. D. *J. Res. Natl. Inst. Stan.* **2008**, *113*, 29.
[48] Sun, C. K. J.; Chen, S. H. *Aiche J* **1985**, *31*, 1510.
[49] Kärger, J. *Micropor. Mesopor. Mater.* **2014**, *189*, 126.
[50] Tzoulaki, D.; Heinke, L.; Lim, H.; Li, J.; Olson, D.; Caro, J.; Krishna, R.; Chmelik, C.; Kärger, J. *Angew. Chem., Int. Ed.* **2009**, *48*, 3525.
[51] Hibbe, F.; Caro, J.; Chmelik, C.; Huang, A. S.; Kirchner, T.; Ruthven, D.; Valiullin, R.; Kärger, J. *J. Am. Chem. Soc.* **2012**, *134*, 7725.

Tables

Table 1: *Specific surface area A_{BET}, specific pore volume V_{pore}, and average pore width d_{pore} determined from N_2-sorption at 77 K and from Hg-intrusion for Pt supported on controlled pore glasses. The platinum content from elemental analysis via ICP-OES is also included.*

Sample	**A_{BET} / (m^2 g^{-1})**	**V_{pore} / (cm^3 g^{-1})**	**d_{pore} / nm**	**Pt-content / wt.-%**
Pt/CPG(4)	95	0.2	4[a)]	2.1
Pt/CPG(10)	130	0.4	10[a)]	2.2
Pt/CPG(80)	80	1.3	60 – 90[b)]	2.4

a) determined from N_2-sorption
b) determined from Hg-intrusion

Figure Captions

Figure 1: *Volume adsorbed (V_{ads}) as a function of relative pressure (p / p_0) from N_2-sorption for Pt supported on controlled pore glass with different pore widths recorded at 77 K (the isotherms are offset by 100 $cm^3 g^{-1}$).*

Figure 2: *Relative differential pore volume ($V_{pore,diff,rel}$), i.e., the differential pore volume divided by the maximum pore volume, as function of pore width (d_{pore}) calculated using the BJH-model on the desorption branch of the nitrogen sorption isotherm for Pt supported on controlled pore glass with different pore widths.*

Figure 3: *Relative volume (V_{rel}) and volume intruded (V_{int}) as a function of pore width (d_{pore}) for the Hg-intrusion profile and pore width distribution histogram of Pt/CPG(80).*

Figure 4: *SEM-micrographs of the catalysts Pt/CPG(4) (top), Pt/CPG(10) (middle) and Pt/CPG(80) (bottom).*

Figure 5: *Toluene conversion $X_{Toluene}$ as a function of reaction time (t) for the hydrogenation of toluene using Pt supported on controlled pore glasses with different pore widths (T = 373 K, p_{H_2} = 50 bar, $c_{toluene}$ = 1.60 mol l^{-1}, solvent: n-hexane (V = 75 cm^3), m_{cat} = 150 mg, stirring rate = 1300 min^{-1}).*

Figure 6: *Initial reaction rate (r_0) as a function of average grain size (d_{grain}) for the hydrogenation of toluene using Pt/CPG(4) and Pt/CPG(10) (T = 373 K, p_{H_2} = 50 bar, $c_{toluene}$ = 1.60 mol l^{-1}, solvent: n-hexane (V = 75 cm^3), m_{cat} = 150 mg, stirring rate = 1300 min^{-1}).*

Figure 7: *Effectiveness factor (η) and Thiele modulus (θ) as a function of average grain size (d_{grain}) for the hydrogenation of toluene using Pt/CPG(4) and Pt/CPG(10) (T = 373 K, p_{H_2} = 50 bar, $c_{toluene}$ = 1.60 mol l^{-1}, solvent: n-hexane (V = 75 cm^3), m_{cat} = 150 mg, stirring rate = 1300 min^{-1}).*

Figure 8: *Reaction scheme for the hydrogenation of alkyl substituted benzenes over Pt supported on controlled pore glasses (Pt/CPG).*

Figure 9: *Initial reaction rate (r_0) for the hydrogenation of toluene, m-xylene, mesitylene and 1,3,5-triisopropyl benzene as a function of their critical molecule diameter (d_{crit}) over the catalysts Pt/CPG(80) and Pt/CPG(10), respectively (T = 373 K, p_{H_2} = 50 bar, $c_{aromatic}$ = 1.60 mol l^{-1}, solvent: n-hexane (V = 75 cm^3), m_{cat} = 150 mg, stirring rate = 1300 min^{-1}).*

Figure 10: *Effective diffusion coefficients (D_{eff}) determined using PFG-NMR for the catalyst Pt/CPG(10) at temperatures (T) between 313 and 373 K.*

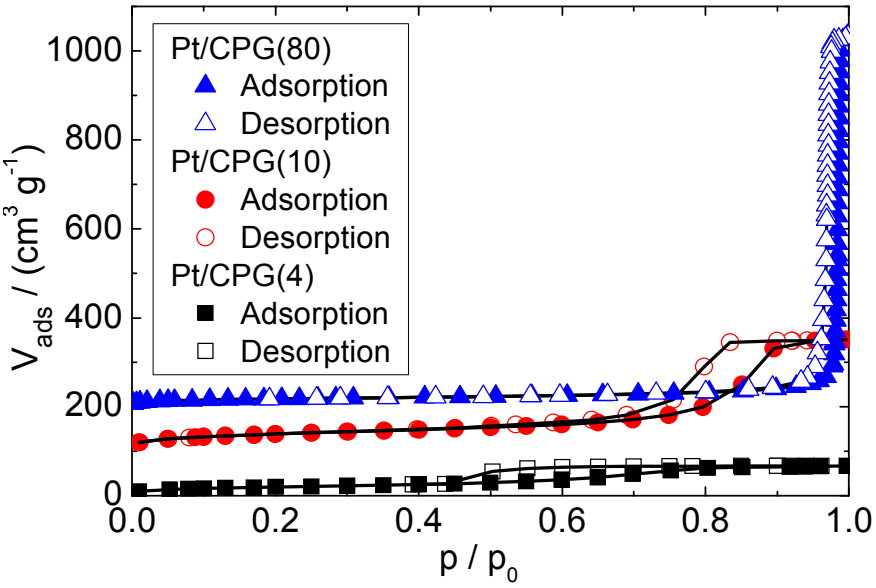

Figure 1: *Volume adsorbed (V_{ads}) as a function of relative pressure (p / p_0) from N_2-sorption for Pt supported on controlled pore glass with different pore widths recorded at 77 K (the isotherms are offset by 100 $cm^3 g^{-1}$).*

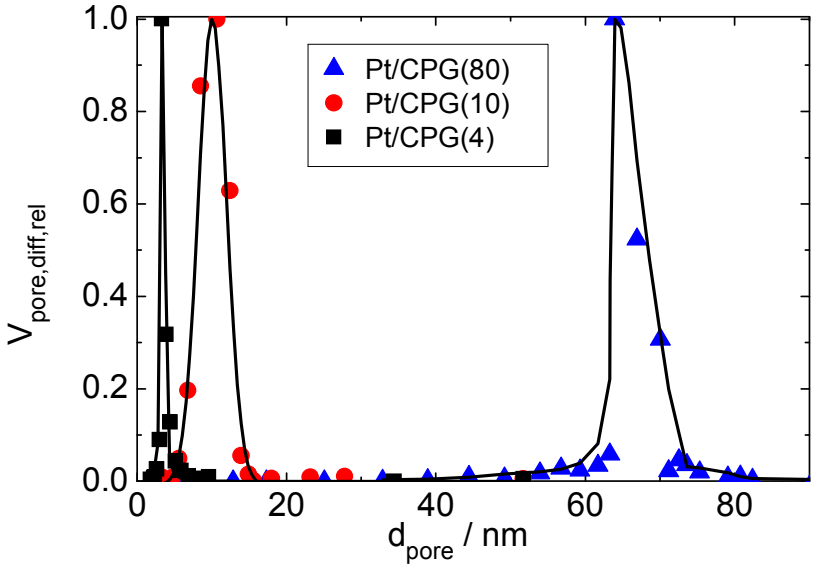

Figure 2: *Relative differential pore volume ($V_{pore,diff,rel}$), i.e., the differential pore volume divided by the maximum pore volume, as function of pore width (d_{pore}) calculated using the BJH-model on the desorption branch of the nitrogen sorption isotherm for Pt supported on controlled pore glass with different pore widths.*

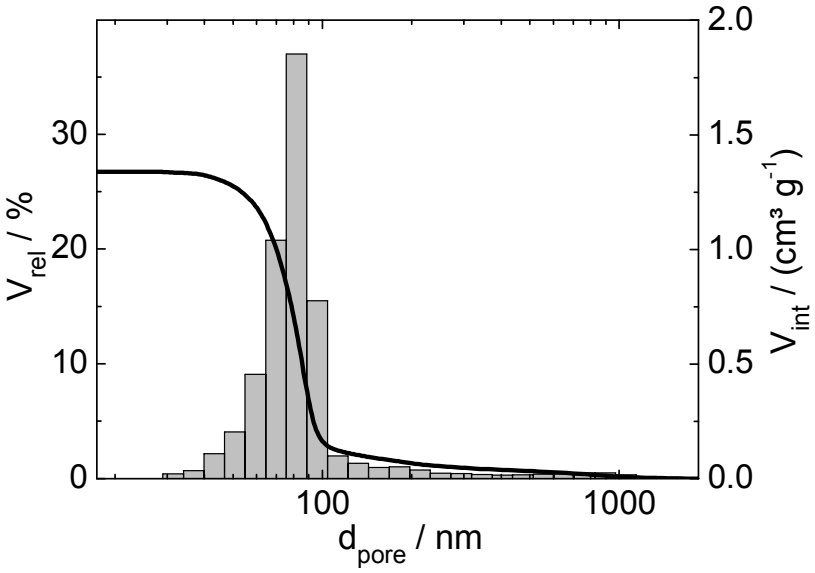

Figure 3: *Relative volume (V_{rel}) and volume intruded (V_{int}) as a function of pore width (d_{pore}) for the Hg-intrusion profile and pore width distribution histogram of Pt/CPG(80).*

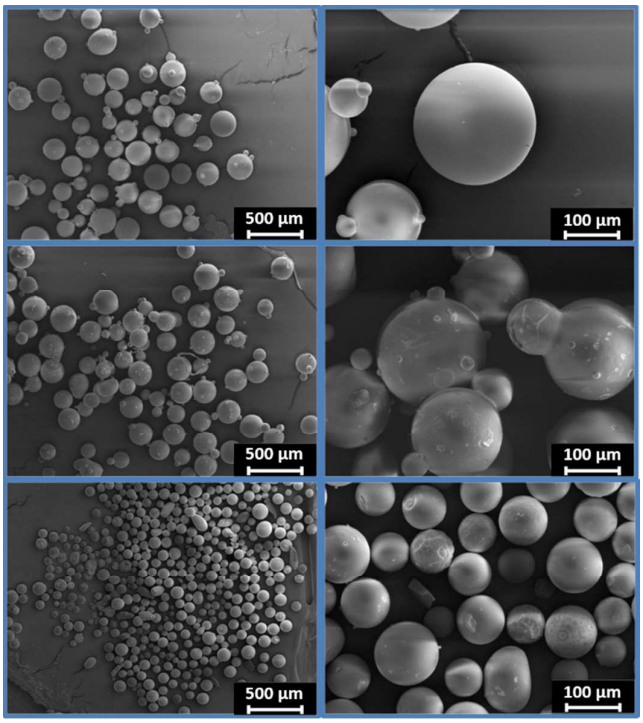

Figure 4: *SEM-micrographs of the catalysts Pt/CPG(4) (top), Pt/CPG(10) (middle) and Pt/CPG(80) (bottom).*

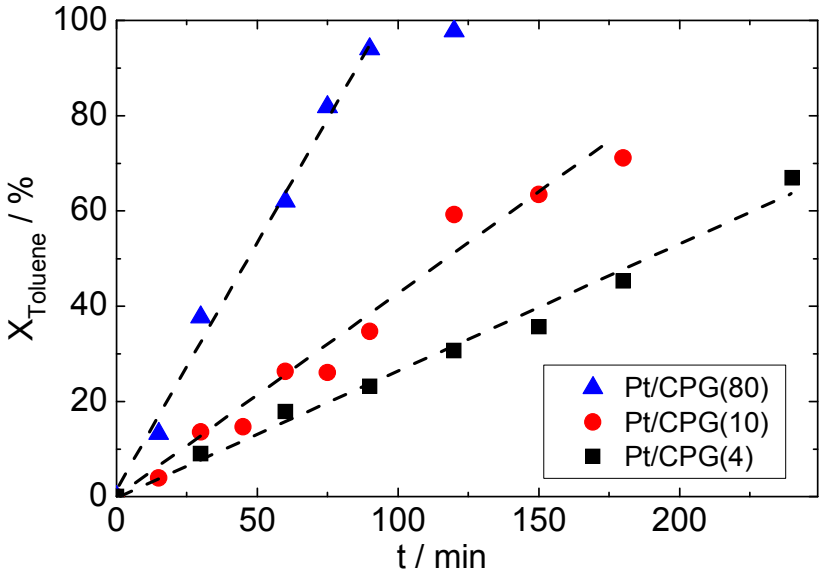

Figure 5: *Toluene conversion $X_{Toluene}$ as a function of reaction time (t) for the hydrogenation of toluene using Pt supported on controlled pore glasses with different pore widths (T = 373 K, p_{H_2} = 50 bar, $c_{toluene}$ = 1.60 mol l^{-1}, solvent: n-hexane (V = 75 cm^3), m_{cat} = 150 mg, stirring rate = 1300 min^{-1}).*

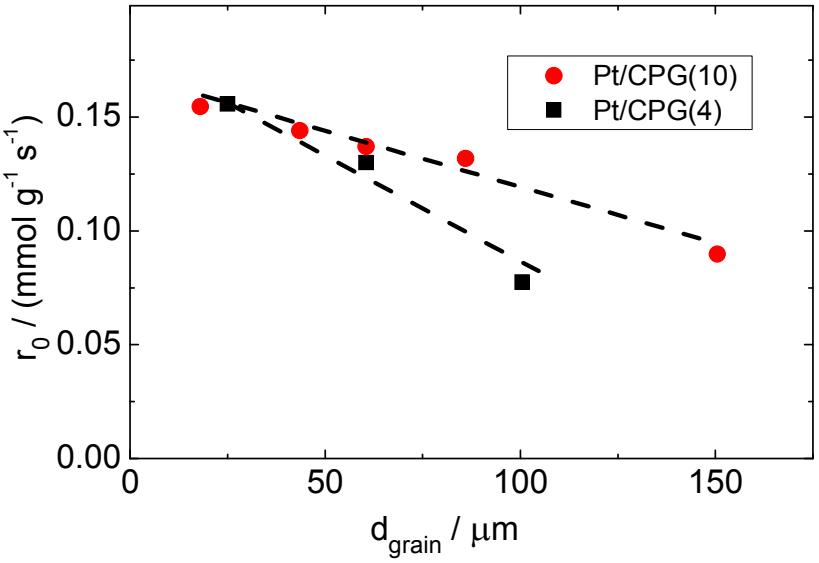

Figure 6: *Initial reaction rate (r_0) as a function of average grain size (d_{grain}) for the hydrogenation of toluene using Pt/CPG(4) and Pt/CPG(10) (T = 373 K, p_{H_2} = 50 bar,*

$c_{toluene}$ = 1.60 mol l^{-1}, solvent: n-hexane (V = 75 cm^3), m_{cat} = 150 mg, stirring rate = 1300 min^{-1}).

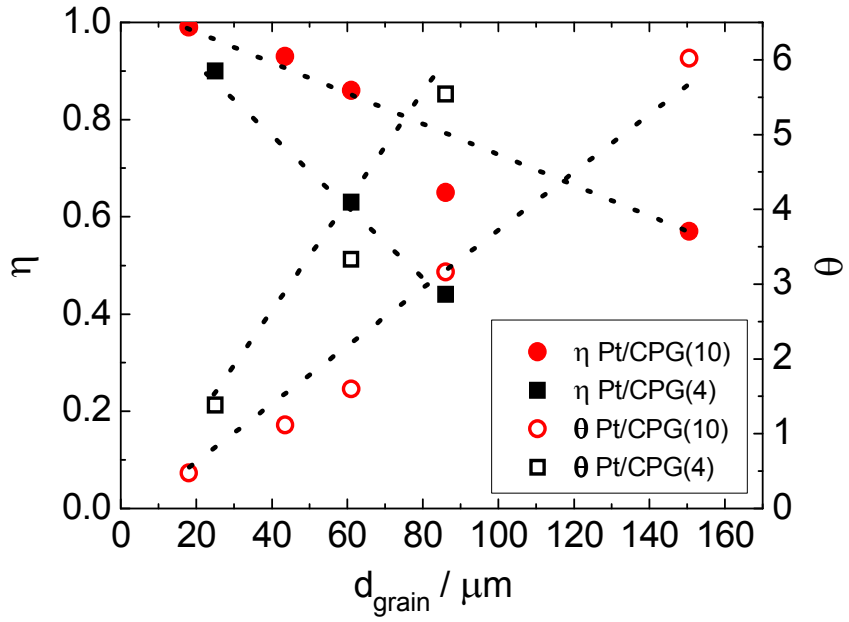

Figure 7: *Effectiveness factor (η) and Thiele modulus (θ) as a function of average grain size (d_{grain}) for the hydrogenation of toluene using Pt/CPG(4) and Pt/CPG(10) (T = 373 K, p_{H_2} = 50 bar, $c_{toluene}$ = 1.60 mol l^{-1}, solvent: n-hexane (V = 75 cm^3), m_{cat} = 150 mg, stirring rate = 1300 min^{-1}).*

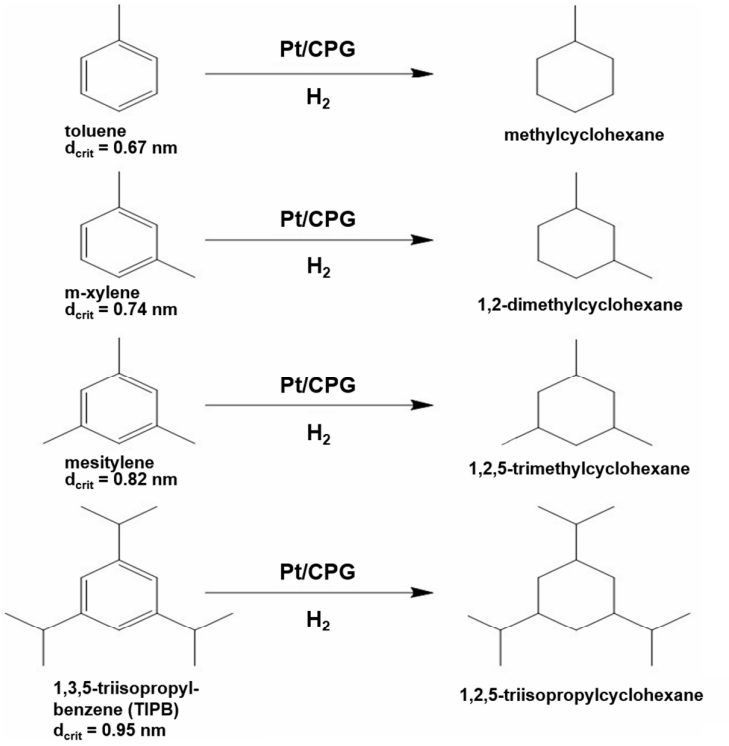

Figure 8: *Reaction scheme for the hydrogenation of alkyl substituted benzenes over Pt supported on controlled pore glasses (Pt/CPG).*

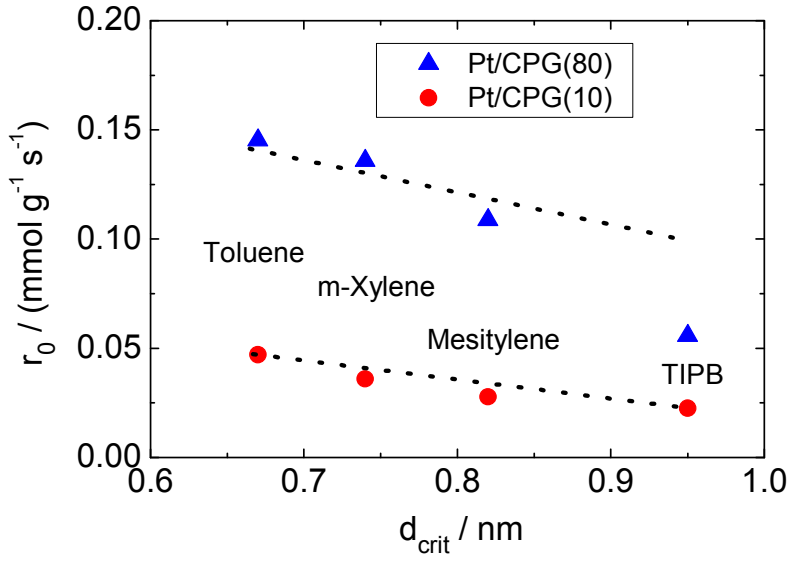

Figure 9: *Initial reaction rate (r_0) for the hydrogenation of toluene, m-xylene, mesitylene and 1,3,5-triisopropyl benzene as a function of their critical molecule diameter (d_{crit}) over the catalysts Pt/CPG(80) and Pt/CPG(10), respectively (T = 373 K, p_{H_2} = 50 bar, $c_{aromatic}$ = 1.60 mol l^{-1}, solvent: n-hexane (V = 75 cm^3), m_{cat} = 150 mg, stirring rate = 1300 min^{-1}).*

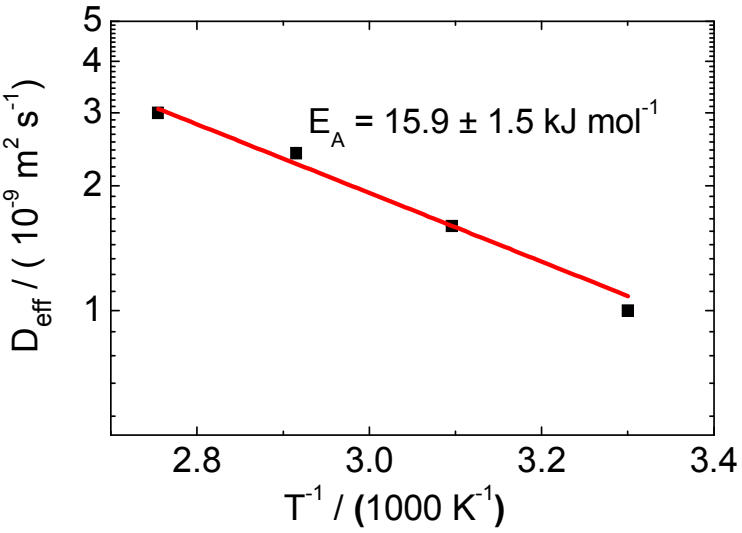

Figure 10: *Effective diffusion coefficients (D_{eff}) determined using PFG-NMR for the catalyst Pt/CPG(10) at temperatures (T) between 313 and 373 K.*